EOS, TRANSACTIONS, AMERICAN GEOPHYSICAL UNION

EOS

VOLUME 74, NUMBER 3

JANUARY 19, 1993

PAGES 33–40

Los Angeles Fires Seen from Space

PAGES 33, 37–38

Bénédicte Dousset, Pierre Flament, and Robert Bernstein

Hundreds of fires were set in Los Angeles following the verdict of Rodney G. King versus the Los Angeles Police Department on April 29, 1992. These fires were of sufficient intensity and extent to be imaged at 1-km resolution by the Advanced Very High Resolution Radiometer (AVHRR) aboard the polar-orbiting satellites operated by the National Oceanic and Atmospheric Administration (see *VanWoert et al.* [1992] for an overview of the characteristics of the AVHRR instrument). Here we present a thermal infrared image taken the first night of the riots, compare it with an image taken several years earlier but typical of this area, and discuss the relationships with the land cover observed in a 20-m resolution image from the French satellite SPOT (Système Probatoire pour l'Observation de la Terre).

The 3.7-μm thermal infrared image taken on April 30 at 3:47 PDT (approximately 10 hours after the start of the riots) is shown in Figure 1a. An exceptionally large thermal anomaly, extending over more than 85 km^2 and saturating at 48.6°C on a few pixels, is seen near the center of the image (the warm sector at the bottom left is the ocean, which is warmer than the land at night). This thermal anomaly corresponds to south central Los Angeles, where an average of three new fires were started each minute during the 3 hours preceding the image. In contrast, surface temperature is fairly uniform in thermal infrared images taken under normal conditions. Figure 1b shows an image from a series taken in August 1984 and 1985. Slight increases of ~2°C are seen over the industrial zone of El Segundo near the coast, and over downtown Los Angeles, a so-called "urban heat island" related to the lower moisture availability of the soil in these areas [*Oke*, 1978].

The positions of these thermal anomalies with respect to urban features are illustrated in the SPOT image (Figure 1c). Land covers were classified using the green and near-infrared channels, which best discriminate between building structures and vegetation [cf. *Dousset*, 1991]. Major boulevards and avenues (for example, Wilshire, Pico, Manchester) are revealed by industrial/commercial buildings bordering them, coded in red. Interstate highways (such as I-10 and I-405), which are not bordered by constructions, are barely visible. Residential blocks, identified by their vegetation, are coded in blue. Irrigated golf courses, such as the Los Angeles Country Club on Wilshire Boulevard and the Hillcrest Country Club on Pico Boulevard, are coded in green. The low-vegetation area in downtown Los Angeles is seen as the large red patch in the northeast of the image. Other low-vegetation areas are the industrial zone of El Segundo and LAX airport near the ocean. The boundaries of these low-vegetation areas correspond closely to the urban heat islands seen in Figure 1b. The large thermal anomaly seen in Figure 1a, however, is located southwest of downtown Los Angeles, an area that is cooler under normal conditions.

The temperature variations are best quantified in the north to south section shown in Figure 2. For the "normal" image (bottom panel), the brightness temperatures are fairly uniform in the 3.7-μm and 10.8-μm channels, with a slight increase from 13°C to 15°C as the section grazes the heat island of downtown Los Angeles at 10 km. In the image taken on the night of the fire (central panel), the variations of brightness temperatures in the 10.8-μm and 12.0-μm channels mimic those seen in the normal image, also with a slight maximum near downtown Los Angeles. The variations of brightness temperature in the 3.7-μm channel are drastically different, with an increase of several degrees over the fire areas, and a peak to 45°C at 19 km over Manchester Avenue. The difference between the anomalous 3.7-μm channel and the 10.8-μm channel is contoured on figures 1a and 1c.

Figure 3 shows how the AVHRR sensor is able to detect fires of subpixel size. The spectral brightness of a normal ground pixel at a uniform temperature of 13°C follows a Planck function peaking near 10 μm (curve A). Three independent measurements of brightness temperature are obtained from the three AVHRR infrared channels, which, except for measurement noise and atmospheric effects, yield the same value of surface temperature for a uniform pixel. The spectral brightness of a burning building also follows a Planck function but peaks at shorter wavelengths, according to Wien's law (curves B and C). The spectral brightness integrated over a pixel with a few isolated fires will thus follow a hybrid function (thick curve), which is not a Planck function, from which different brightness temperatures are inferred for each spectral channel. The 3.7-μm channel is most sensitive; the 10.8-μm channel is much less sensitive.

Given brightness temperatures T_i measured in two channels (that is, 3 and 4) and the background temperature T_b of an adjacent (uniform) pixel, approximating the spectral response of these (narrow) channels as gates and linearizing the Planck function in these gates, in principle, it is possible to estimate both fire temperature T_f and fraction of pixel burning p, by solving the system

$$B(\lambda_i,T_i) = p\,B(\lambda_i,T_f) + (1-p)B(\lambda_i,T_b) \quad (1)$$

where $B(\lambda,T)$ is the Planck function, and $i = 3,4$; this was first proposed by *Dozier* [1981] and *Matson and Dozier* [1981]. In the present case, the ~31°C step seen in the 3.7-μm channel between 19 and 20 km corresponds to a ~1.0±0.1°C step in the 10.8-μm channel; solving (1) with these values yields a coverage $p = 0.095\pm0.015\%$ and a pixel-average fire temperature $T_f = 425\pm20$°C. The 10.8-μm-channel anomaly of other pixels is buried in the radiometer noise, making a strict pixel-by-pixel solution of (1) impossible. However, if the fire temperature T_f is known or assumed a priori, the areal fraction burning can be estimated from the 3.7-μm channel alone.

Fire temperature is a poorly known and difficult to measure quantity. *Robinson* [1991] reviews measurements made under laboratory conditions and cites a minimum of 300°C to sustain flaming combustion in cellulosic fuels and 500°–600°C for glowing combustion in charcoal. Thick wood flames burn at ~1000°C. If most of the burning areas consist of smoldering collapsed roofs, the average fire temperature $T_f = 425$°C estimated above may not be unrealistic. The fraction of burning area is plotted in Figure 2c, assuming a constant fire temperature $T_f = 425$°C. It peaks at 0.095% over Manchester Avenue, indicating that about 950 m^2 may have been actively burning in this 1-km^2 pixel at the time of the image.

Bénédicte Dousset and Pierre Flament, School of Ocean and Earth Sciences and Technology, University of Hawaii at Manoa, 1000 Pope Road, Honolulu, HI 96822; Robert Bernstein, SeaSpace, 3655 Nobel Drive, Suite 160, San Diego, CA 92122

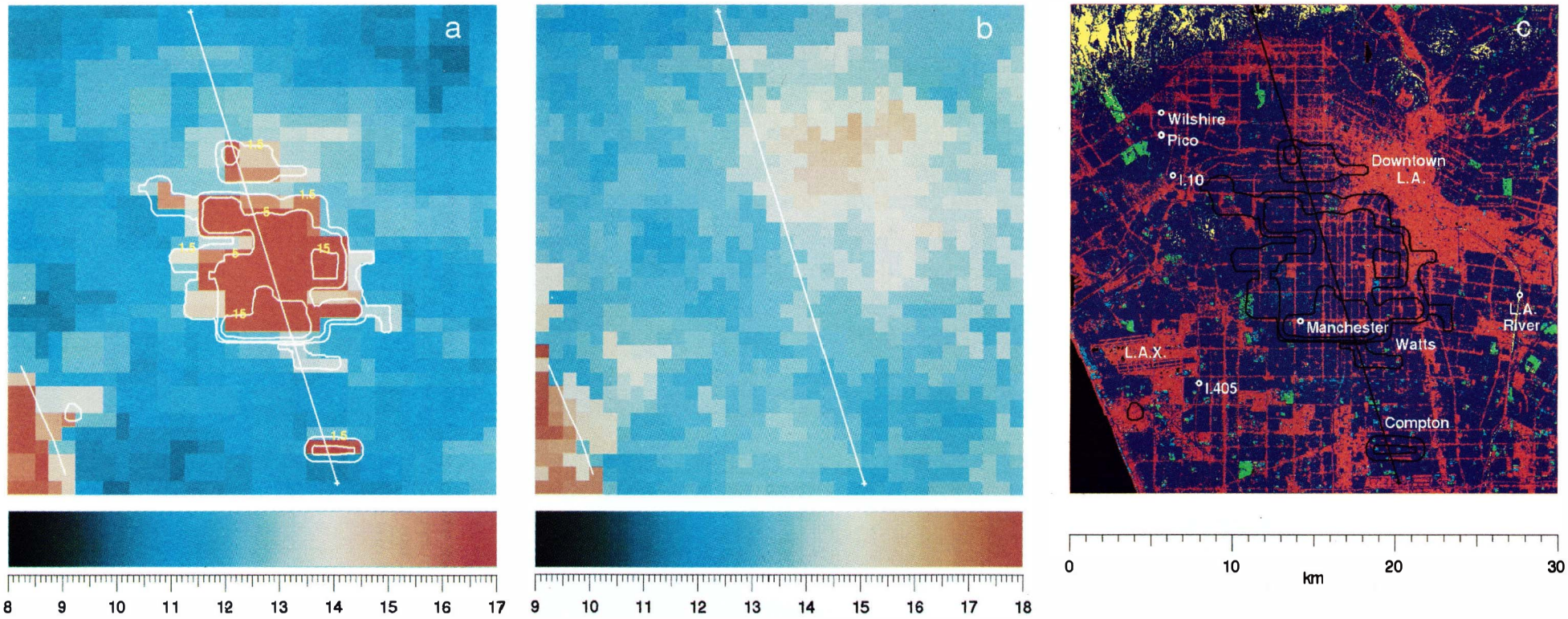

Fig. 1. (a) A 3.7-μm brightness temperature image from the NOAA-11 AVHRR on April 30, 1992, at 3:47 PDT, about 10 hours after the onset of the arson fires. (b) A 3.7-μm image from the NOAA-9 AVHRR during normal conditions, on August 2, 1985, at 4:22 PDT. (c) Pseudo-color land cover classification on June 15, 1985, based on a multispectral SPOT image (copyright CNES/SPOT Image Corporation, 1985). The section plotted in Figure 2 and the contours of temperature difference between the 3.7-μm and 10.8-μm AVHRR channels are overlaid on (a) and (c). North is up. Temperatures are in degrees Celsius.

The conditions for fire detection over a background at 13°C are shown in Figure 4. There is an approximate inverse relationship between fire temperature and fraction covered for a given brightness temperature anomaly. The sensitivity of the 3.7-μm channel to small fires is, in fact, astounding. A fire at T_f = 425°C covering 2 X 10^{-3} % of a pixel, or just 20 m^2, will cause a temperature anomaly of 1°C, well above the radiometer noise. The sensitivity of the AVHRR has been documented for a variety of fires, including forest and agricultural fires [*Muirhead and Cracknell*, 1985; *Matson et al.*, 1987; *Lee and Tag*, 1990], gas and oil well flares [*Matson and Dozier*, 1981; *Muirhead and Cracknell*, 1984], industrial hot spots [*Matson and Dozier*, 1981], and localized urban fires following the 1989 San Francisco earthquake [*Lee and Tag*, 1990].

The extreme sensitivity of the 3.7-μm channel is well illustrated in Figure 1a. The contours of temperature anomaly correspond closely to the areas where fires were reported. The northernmost anomaly is at the intersection of Venice Boulevard and Western Avenue in Koreatown, where many stores were burning. Manchester Avenue, one of the hardest hit, appears as a temperature maximum. The anomaly protruding to the northwest corresponds to burning stores off Crenshaw Boulevard. The isolated but intense hot spot to the south of the image is the Compton Center Mall, where a department store was burning. The small hot spot near the ocean corresponds to the temperature anomaly of an oil refinery in El Segundo.

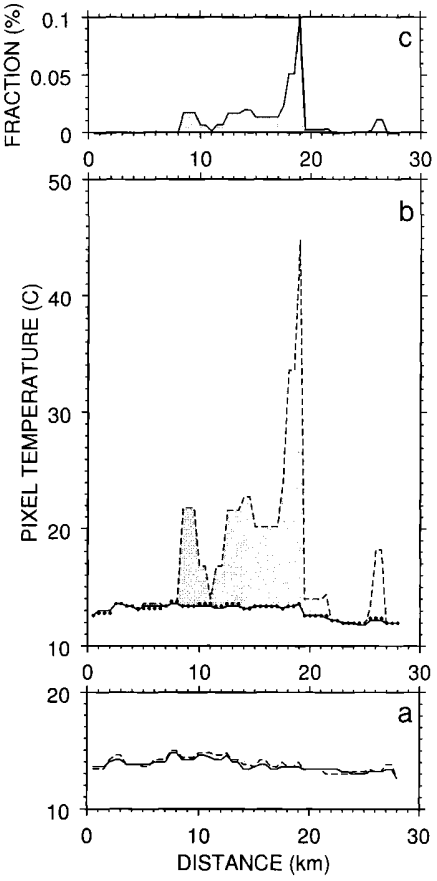

Fig. 2. North to south section through the images, along the line shown in Figure 1. (a) Brightness temperatures on August 2, 1985, at 4:22 PDT, at 3.7 μm (dashed) and 10.8 μm (solid). (b) Brightness temperatures on April 30, 1992, at 3:47 PDT, at 3.7 μm (dashed), 10.8 μm (solid), and 12.0 μm (dotted). (c) Areal pixel fraction covered by smoldering fires assumed at 425°C needed to account for the observed 3.7-μm-channel anomalies.

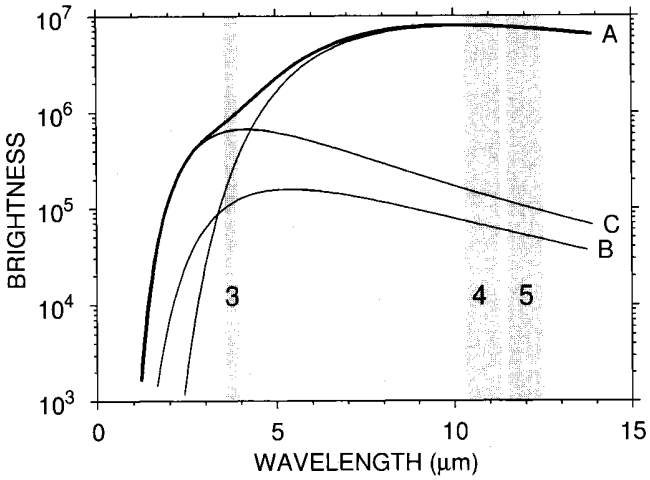

Fig. 3. (a, thin line) Spectral brightness (in W m^{-3} Sr^{-1}) of the ground at a uniform temperature of 13°C. (b) Contribution to the brightness of smoldering fires at 250°C covering 0.1% of the pixel. (c) Contribution to the brightness of flaming fires at 425°C covering 0.1% of the pixel. The thick line illustrates the spectral brightness that would be observed for a combination of (a) and (c). The infrared spectral channels (3, 4, and 5) of the AVHRR are stippled.

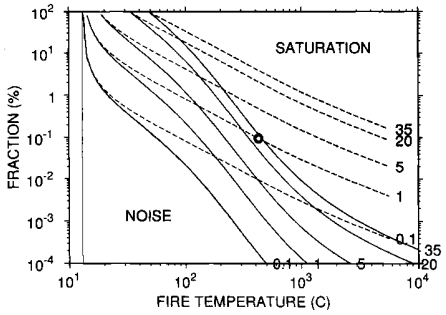

Fig. 4. Conditions for fire detection in the 3.7-μm channel: Relationships between fire temperature and fraction of pixel covered, for brightness temperature anomalies ΔT = 0.1, 1, 5, 20 and 35°C, assuming a uniform background temperature of 13°C. Conditions below the noise level of the AVHRR, ΔT < 0.1°C, and above saturation, T > 48°C or ΔT > 35°C, are shaded. The dashed lines show similar relationships in the less sensitive 10.8-μm channel; equation (1) can be solved for both p and T_f only in the unshaded sector above the 0.1°C dashed line. The conditions for the Manchester Avenue pixel are marked with a solid circle.

The radiometric temperatures used in this discussion were computed assuming that the surface is a perfect blackbody and that the atmosphere is perfectly transparent. They differ slightly from actual surface temperatures because most materials found in urban areas have an emissivity smaller than one, and because water vapor and aerosols (mainly smoke) absorb some of the upwelling radiation. The implementation of temperature corrections, however, is beyond the scope of this note.

Typical emissivities are given by *Buetner and Kern* [1965] and *Arnfield* [1982]. The average emissivity of a commercial/residential block, consisting mainly of vegetation (0.975), asphalt (0.956), shingle roofs (0.962), and concrete (0.966), is about 0.96–0.97. This would correspond to a temperature error of -1.8 to -2.4°C. This error is partially compensated by the downwelling sky radiation reflected by the surface. The emissivity of the fires can be taken as that of a blackbody.

The mean difference between the 10.8-μm channel, less absorbed by water vapor, and the 12.0-μm channel, more absorbed, is about 0.1°C (Figure 2b). This small difference illustrates the low water vapor content found in dry subtropical regions such as Southern California, resulting in only a few percent absorption of infrared radiation by the intervening atmosphere. In this case, a two-channel atmospheric correction [*Deschamps and Phulpin*, 1980; *McClain*, 1985] would be less than 0.3°C and could be neglected to first approximation.

The properties of urban fires were reviewed by the *National Research Council* [1985], in the context of a major nuclear exchange. Smoke aerosols from burning wood and plastics have a mass-median radius of the order of 0.2–0.6 μm; their specific extinction cross section is 4–9 m^2 g^{-1} in the visible, and an order of magnitude smaller in the thermal infrared. The combustible mass of single-story light commercial or residential buildings is typically 50 kg m^{-2}, and about 3–6% of the combustible mass is converted into smoke within a few hours.

The fraction of area burning over the section shown in Figure 2c has a median of 0.01%. Assuming a burn-down time of 6 hours for buildings, a typical wind of 5 m s^{-1} mixing and advecting smoke away from the 10-km wide area, and taking middle values for the parameters given above, the smoke concentration would be ~2 X 10^{-6} kg m^{-2}. Multiplying by the specific extinction cross section yields an optical depth in the thermal infrared of ~10^{-2}. This would corre-

spond to one percent absorption of infrared radiation, smaller than the emissivity error.

The analysis presented here clearly demonstrates that real-time AVHRR imagery, providing synoptic views of the situation using minimum manpower, would be a valuable new tool for assisting fire-fighting efforts in case of major disasters. The importance of such imagery would be greatest when fire-stricken areas are spread over considerable distances, as well as when traditional communications channels such as telephone or radio-telephone networks may be saturated or inoperative. The advent of low-cost portable satellite receiving and processing systems brings this technology within reach of civil defense departments.

Acknowledgments

We would like to thank A. Clarke and an anonymous referee for their comments on atmospheric absorption by aerosols, and W. Cass, of the Los Angeles City Fire Department, for helpful information on the characteristics of the fires. The AVHRR images were received in San Diego and were analyzed at the University of Hawaii Satellite Oceanography Laboratory, using TeraScan systems developed through the efforts of Sea-Space staff members. The plotting program *gri* by D. Kelley (available through anonymous ftp to cs.dal.ca) was used for figures 2–4, and the image composition program *ice* by R. Davis (available through anonymous ftp to eo.soest.hawaii.edu) was used to assemble Figure 1. Contribution number 3069 of the School of Ocean and Earth Sciences and Technology, University of Hawaii.

References

Arnfield, A. J., An approach to the estimation of the surface radiative properties and radiation budget of cities, *Phys. Geogr., 3*, 97, 1982.

Buettner, K. J. K., and C. D. Kern, The determination of infrared emissivities of terrestrial surfaces, *J. Geophys. Res., 70*, 1329, 1965.

Deschamps, P. Y., and T. Phulpin, Atmospheric corrections of infrared measurements of sea surface temperature using channels at 3.7, 11 and 12 micrometers, *Boundary Layer Meteorol., 18*, 131, 1980.

Dousset, B., Surface temperature statistics over Los Angeles: The influence of land use, in *Proceedings of the International Geoscience and Remote Sensing Symposium, Helsinki, 1991*, pp. 367–371, I.E.E.E., New York, 1991.

Dozier, J., A method for satellite identification of surface temperature fields of subpixel resolution, *Remote Sens. Environ., 11*, 221, 1981.

Lee, T. F., and P. M. Tag, Improved detection of hotspots using the AVHRR 3.7-μm channel, *Bull. Am. Meteorol. Soc., 71*, 1722, 1990.

Matson, M., and J. Dozier, Identification of subresolution high temperature sources using a thermal IR sensor, *Photogramm. Eng. Remote Sens., 47*, 1311, 1981.

Matson, M., G. Stephens, and J. Robinson, Fire detection using data from the NOAA-N satellites, *Int. J. Remote Sens., 8*, 961, 1987.

McClain, E. P., W. G. Pichel, and C. C. Walton, Comparative performance of AVHRR-based multichannel sea surface temperatures, *J. Geophys. Res., 90*, 11,587, 1985.

Muirhead, K., and A. P. Cracknell, Identification of gas flares in the North Sea using satellite data, *Int. J. Remote Sens., 5*, 199, 1984.

Muirhead, K., and A. P. Cracknell, Straw burning over Great Britain detected by AVHRR, *Int. J. Remote Sens., 6*, 827, 1985.

National Research Council, *The Effects on the Atmosphere of a Major Nuclear Exchange*, pp. 1–193, National Academy Press, Washington, D.C., 1985.

Oke, T. R., *Boundary Layer Climates*, 364 pp., Methuen & Co., London, 1978.

Robinson, J. M., Fire from space: Global fire evaluation using infrared remote sensing, *Int. J. Remote Sens., 12*, 3, 1991.

VanWoert, M. L., R. H. Whritner, D. E. Waliser, D. H. Bromwich, and J. C. Comiso, ARC: Source of multisensor satellite data for polar science, *Eos Trans. AGU, 73*, 65, 1992.